A theory of the MJO horizontal scale

Da Yang[1] and Andrew P. Ingersoll[1]

[1]Division of Geological and Planetary Sciences, California Institute of Technology, Pasadena, California, USA

Abstract Here we ask, what controls the horizontal scale of the Madden-Julian Oscillation, i.e., what controls its zonal wave number k? We present a new one-dimensional (1D) β-plane model that successfully simulates the MJO with the same governing mechanism as the 2D shallow water model of Yang and Ingersoll (2013). Convection is parameterized as a short-duration localized mass source that is triggered when the layer thickness falls below a critical value. Radiation is parameterized as a steady uniform mass sink. Both models tend toward a statistically steady state—a state of radiative-convective equilibrium, not just on a global scale but also on the scale of each MJO event. This gives $k \sim (S_c/c)^{1/2}$, where S_c is the spatial-temporal frequency of convection events and c is the Kelvin wave speed. We offer this scaling as a prediction of how the MJO would respond to climate change.

1. Introduction

The Madden-Julian Oscillation (MJO) is the dominant intraseasonal variability in the tropics. It is a slowly eastward propagating (~ 5 m/s) planetary-scale envelope of organized convection [*Madden and Julian*, 1972, 1994; *Zhang*, 2005]. Within the large-scale envelope, there are both westward- and eastward-moving fine-scale structures [*Nakazawa*, 1988].

Many previous studies consider the MJO as a large-scale unstable mode in the tropics, which is often referred to as the moisture mode. The moisture mode arises from positive feedbacks between precipitation and the source of moist static energy [e.g., *Neelin and Yu*, 1994; *Sobel et al.*, 2001; *Fuchs and Raymond*, 2002, 2005, 2007; *Bretherton et al.*, 2005; *Maloney*, 2009; *Raymond and Fuchs*, 2009; *Andersen and Kuang*, 2012]. Consistent with treating the MJO as a large-scale low-frequency mode, convection is usually treated as a quasi-equilibrium (QE) process [*Emanuel et al.*, 1994]. In the soft QE context, i.e., finite time-scale convection, high-frequency waves are damped the fastest due to the moist convective damping effect [*Emanuel et al.*, 1994]. Therefore, the role of high-frequency waves has not really been evaluated in these theories.

However, there is growing evidence, both in the models and in the observations, suggesting that triggered convection might be important to the MJO. As opposed to QE convection, triggered convection allows the atmosphere to accumulate convective available potential energy (CAPE), and convection is therefore intermittent and energetic. For instance, *Holloway et al.* [2013] find that explicit convection simulations perform better than parameterized simulations in matching the strength and propagation speed of the MJO. Models with a good MJO representation have increased generation of available potential energy and conversion of that energy into kinetic energy. These models also have a more realistic relationship between lower-free-tropospheric moisture and precipitation. *Holloway et al.* [2013] conclude that moisture-convection feedback is a key process for MJO propagation. Here we explore the idea that conversion of CAPE into kinetic energy by triggered convection is the important process. *Zuluaga and Houze* [2013] use radar-reflectivity fields, ECMWF ERA-interim reanalysis data, and three-hourly atmospheric soundings to examine the most extreme convective entities during the Dynamics of the MJO (DYNAMO) field project. Their analyses show that rainfall is intermittent and separated by nonrainy days during active phases of the MJO. They also show that CAPE increases before maximum rainfall accumulation and then decreases. The magnitude of change in CAPE is 200–300 J/kg. This result indicates that triggered convection does happen during the active phase of the MJO. They further propose that the rainfall intermittency is due to high-frequency equatorial waves.

Yang and Ingersoll [2013, hereafter YI13] developed a 2D shallow water model of the MJO that emphasizes the role of triggered convection and high-frequency waves. Convection is parameterized as a short-duration localized mass source and is triggered when the layer thickness falls below a critical value. Radiation is parameterized as a steady uniform mass sink. Over a wide range of parameters, they observed MJO-like signals (Figures 1, 3, and 4 in YI13) similar to the observed MJO in the upper troposphere. Based on their simulation results, YI13 proposed that the MJO could be an interference pattern of the westward and eastward (WIG and

EIG) inertia gravity waves. The propagation speed of the MJO is approximately equal to one half the phase speed difference between the EIG and WIG waves.

In this paper, we further explore the YI13 model and seek a quantitative understanding of what controls the MJO horizontal scale. In section 2, we briefly describe the YI13 model, present the simulation results, and propose a radiative-convective equilibrium (RCE) scaling theory. In section 3, we derive a 1D β-plane model based on the YI13 model and use this 1D model to test the RCE scaling. In section 4, we present our conclusions and plans for future work, and we discuss some possible climatological implications of our results.

2. 2D Shallow Water Model

YI13 used a global 2D shallow water model to simulate the upper troposphere by assuming that the MJO is dominated by the first baroclinic mode in the vertical. Thus, divergence in this model refers to upper level divergence and low-level convergence. Similarly, small layer thickness in the model corresponds to low pressure aloft and high pressure near the surface, implying low average tropospheric temperature.

In YI13, we modify the 2D shallow water equations by adding convective heating q and radiative cooling r in the continuity equation, which is given by

$$\partial_t \phi + \nabla \cdot \left(\vec{V} \phi \right) = q - r. \tag{1}$$

In 1, ϕ is the geopotential, which is gravity times the layer thickness; $\vec{V}$ is the vector velocity, composed of zonal and meridional velocities. In this model, convection is a small-scale mass source and is triggered when ϕ is lower than a threshold ϕ_c. The convective heating is given by:

$$q = \begin{cases} \dfrac{q_0}{\tau_c A_c} \left[1 - \left(\dfrac{\Delta t - \tau_c/2}{\tau_c/2} \right)^2 \right] \left(1 - \dfrac{L^2}{R_c^2} \right), & when \quad \phi < \phi_c \quad 0 < \Delta t < \tau_c, \quad L^2 < R_c^2; \\ 0, & otherwise. \end{cases} \tag{2}$$

Here q_0 is the heating amplitude, τ_c is the convective timescale, and Δt is measured relative to the time when convection is triggered. Each convective event operates in a certain area $A_c = \pi R_c^2$, where R_c is the radius of each convective event. The convective heating will be superposed if one location sits between two separate convection events. Δt is then calculated separately for two events. L is distance from the convective center. Each convection event increases ϕ by an amount $\frac{q_0}{3}$ during its lifetime. The radiative cooling term r removes mass uniformly at a steady rate. In a statistically steady state, ϕ fluctuates around the equilibrium geopotential ϕ_c, and the convective heating balances the radiative cooling over the globe. According to this mass balance, we define the number density of convection S_c, with units number area^{-1} time^{-1}, as follows:

$$S_c = 3r/q_0. \tag{3}$$

We keep the forcing amplitude small, so the fluid dynamics is linear. Then we have four independent parameters in this model, and they are τ_c, R_c, S_c, and the Kelvin wave speed c, defined as $\sqrt{\phi_c}$. The planetary radius a and the rotation rate Ω define the length and time scales of the problem. We systematically vary the first four parameters and explore the parameter dependence of the MJO wave number k, which corresponds to dimensional wavelength $2\pi a/k$.

Figure 1 shows the parameter dependence of k in 10-based log-log plots. Each marker represents one simulation result. To estimate k, we first construct the wave number-frequency diagram (e.g., Figure 3a in YI13). Then we search the wave number that occupies the most spectral power at each frequency in the MJO region, the white box area in Figure 3a of YI13. The wave number of the MJO is the weighted average of these wave numbers. In this study, we draw a wider white box than that in YI13 in both frequency and wave number to include the entire MJO spectral power. $\log k$ increases linearly with $\log S_c$, and the slope is ~ 0.4 (Figure 1a). $\log k$ decreases linearly with $\log c$, and the slope is ~ −0.7 (Figure 1b). $\log k$ increases linearly with $\log R_c$, and the slope is ~ 0.5 (Figure 1c). In Figures 1a, 1b, and 1c, these linear relations suggest power law relations between k and S_c, c, and R_c. These power law relations break down when k gets too small or too large. When k is close to 2, the MJO horizontal scale is large and is limited by the size of the planet. When k is
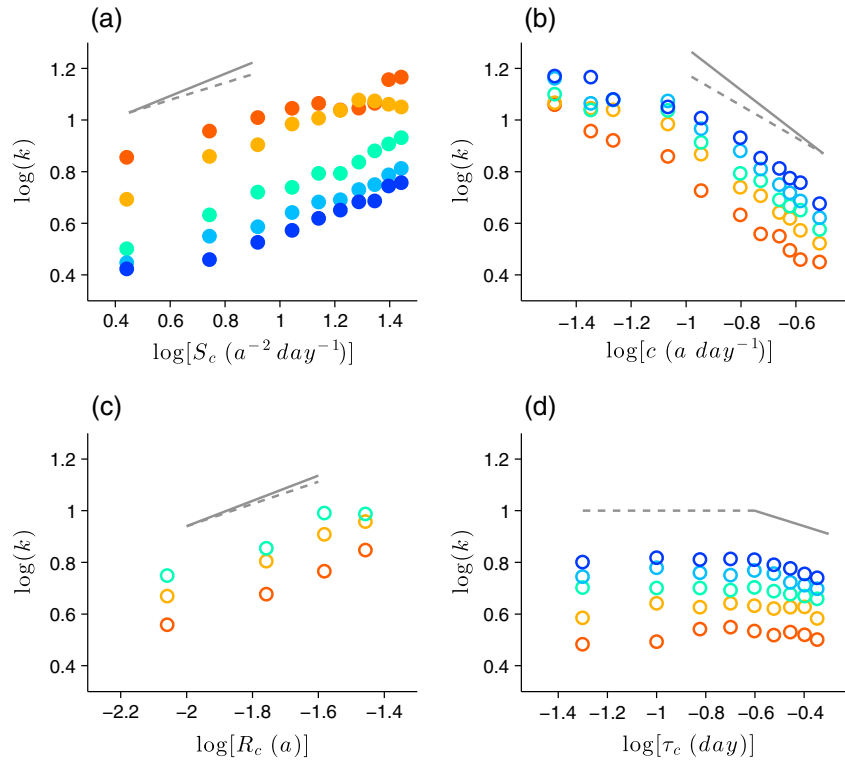
Figure 1. Sensitivity study results in 10-based logarithmic scale. (a) The MJO wave number k vs number density of convection S_c (a^{-2} day^{-1}). Different colors represent simulations with different Kelvin wave speeds. They increase from red to blue, and the values are ~ 3, 6, 12, 16, 19 m s^{-1}. The solid (dashed) line is with the slope of 0.43 (0.33). (b) k vs Kelvin wave speed c (a day^{-1}). The solid (dashed) line has a slope of -0.82 (-0.62). (c) k vs the radius of a convection event R_c (a). The solid (dashed) line has a slope of 0.43 (0.49). (d) k vs τ_c (day). The solid (dashed) line has a slope of -0.3 (0.0). In Figures 1b, 1c, and 1d, colors represent simulations with S_c increasing from red to blue. The values of S_c are ~ (5.6 11.2 16.8 22.4 28.0) a^{-2} day^{-1}.

10 or above, we cannot distinguish one MJO event from another, and k is therefore saturated. In the next section, we construct a 1D model that solves an equatorial channel with large zonal domain and can avoid this problem. Figure 1d shows the k dependence on τ_c. Although we have varied τ_c by one order of magnitude, k does not change much, especially compared to other parameters. Therefore, k has a very weak dependence on τ_c. Since k is a discrete number, there are uncertainties in estimating k, especially when k is small. In Figures 1a, 1b, and 1c, the grey solid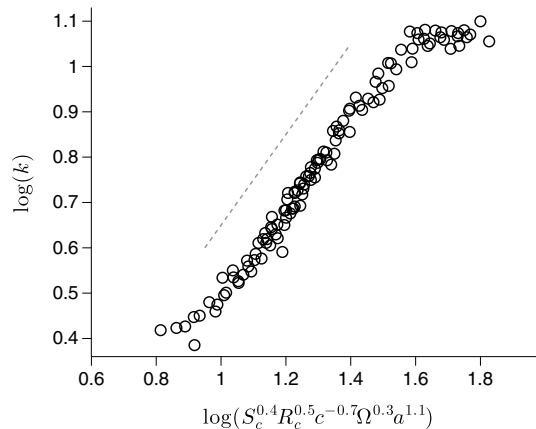 and dashed lines illustrate the largest and smallest slopes calculated using simulations varying the corresponding x axis variable only. This spread in slope is a measure of uncertainties in estimating k.

Figure 2. The proposed scaling relation in a 10-based log-log plot. Each marker represents a simulation result. The dashed line has a slope of 1.

According to our simulation results, we propose an empirical scaling relation between the MJO wave number and the model parameters

$$k = S_c^{0.4} R_c^{0.5} c^{-0.7} \Omega^{0.3} a^{1.1} F(\tau\Omega). \quad (4)$$

The exponents of Ω and a are derived through dimensional analysis, and $F(\tau\Omega) \sim O(1)$. In Figure 2, we plot the simulation results according to 4. Most of the simulation results collapse into one curve. When k is between 2 and 10, this curve is linear and is parallel to the dashed line. Since the dashed line has the slope of 1, it suggests that the proposed scaling fits our simulation results.

Next we propose a simpler scaling that approximately reproduces the empirical scaling in (4). Since S_c is the number of convective events per unit area per unit time, we let each convective event occupy a box in space and time of dimensions $L_z \times L_m \times T$, where $L_z = ak^{-1}$ is the zonal dimension, $L_m \propto R_c$ is the meridional dimension, and $T = ak^{-1}/c$ is the time dimension. This gives

$$k \sim S_c^{0.5} R_c^{0.5} c^{-0.5} a^{1.0} F(\tau\Omega) \sim (S_c R_c/c)^{1/2} a. \tag{5}$$

In effect, we are assuming that each MJO cycle is in RCE. On average, there is $O(1)$ convective event within the box, which is defined partly by the MJO zonal scale L_z and the time it takes a gravity wave to propagate across that scale. We have associated the meridional dimension of the box with the size R_c of an individual convection event, although other interpretations are possible. That assumption has the advantage of giving the same R_c dependence in the two equations, (4) and (5). The MJO envelope is composed of many of these boxes defined above, which give the complex and multiscale structure of the MJO. It is difficult to compare our results with observations, e.g., precipitation inferred from infrared images [*Chen et al.*, 1996], since it is not clear what constitutes an individual event in the sense we are using it. Nevertheless, the scaling of equation (5) is consistent with Figure 1d of YI13, and that figure more or less matches the number of convective events seen in the infrared images.

Equations (4) and (5) are similar. The differences can be attributed to: (1) Each MJO event might not be in RCE because of interference between the MJO and midlatitude activity, e.g., Rossby waves excited by convection at midlatitudes; (2) k is discrete, and the estimation of k is reliable only if $k \gg 1$. This situation, however, is never met, because k gets saturated when $k \to 10$. In other words, there are uncertainties when estimating k. To test this RCE scaling, we construct a 1D β-plane model. This 1D model does not have a meridional scale or interference from higher latitudes. Also, it has a much larger domain, so the uncertainties in estimating k are smaller.

3. 1D β-Plane Model

Since we keep the forcing amplitude small, and the MJO is confined to tropics, the linearized β-plane model keeps all the essential dynamics of the YI13 model. Following *Matsuno* [1966], we start with the 2D shallow water equations on an equatorial β-plane. To construct the 1D model, we assume the meridional structure of zonal wind U, meridional wind V, and geopotential ϕ as follows:

$$U = (u + by^2)\exp(-\beta y^2/2c), \tag{6}$$

$$V = vy\exp(-\beta y^2/2c), \tag{7}$$

$$\phi = (f + gy^2)\exp(-\beta y^2/2c). \tag{8}$$

u, v, b, f, and g are functions of x and t. After substitution into the equatorial β-plane equations, the b variable drops out, and we are left with four equations that exactly capture the lowest symmetric meridional modes—the Kelvin wave and the $n = 1$ equatorial Rossby and inertia gravity (IG) waves. We use $(c/\beta)^{1/2}$ as our length scale, and $(\beta c)^{-1/2}$ as our timescale. The nondimensional model equations are

$$\hat{u}_{\hat{t}} = -\hat{f}_{\hat{x}}, \tag{9}$$

$$\hat{v}_{\hat{t}} = -\hat{u} - 2\hat{g} + \hat{f}, \tag{10}$$

$$\hat{f}_{\hat{t}} = -\hat{u}_{\hat{x}} - \hat{v} - \hat{r} + \hat{q}, \tag{11}$$

$$\hat{g}_{\hat{t}} = -\hat{g}_{\hat{x}} + \hat{v} - \hat{r} + \hat{q}, \tag{12}$$

where $\hat{\cdot}$ represents nondimensional variables. Here $\hat{r}$ is the radiative cooling, and $\hat{q}$ is the convective heating. The radiation and convection parameterizations are the same as in the YI13 model. Convection is triggered when the geopotential $\hat{f} + \hat{g}$ is lower than a threshold. The convective timescale is $\hat{\tau}_c$, and the size of each convection event is $\hat{R}_c$. In this 1D model, there are three nondimensional parameters, $\hat{\tau}_c$, $\hat{R}_c$, and $\hat{S}_c = \frac{9}{8}\frac{\hat{r}}{\hat{q}_0}$, where the proportionality comes from the temporal and spatial integration over the duration and size of each convective storm. Since there is no meridional dimension, the units of S_c are number length^{-1} time^{-1}, and R_c is the width of the convection in the zonal direction. The domain size of this model is 400 in the nondimensional units of the equatorial Rossby radius $\sqrt{c/\beta}$. This domain size is about 10 times larger than the Earth's equatorial circumference in the dimensional sense. In the previous section, wave number is a nondimensional quantity scaled by
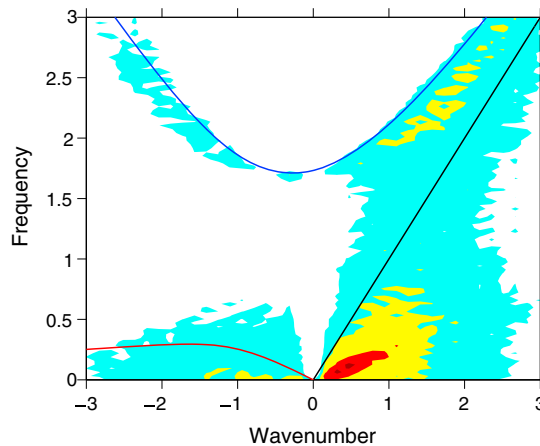
Figure 3. The power spectrum of $\hat{u}$ from the 1D β-plane model. The contours show the power spectral density in intervals of log to the base 10. Red represents high-power density, and blue represents low-power density. Red, blue, and black lines denote dispersion curves of Rossby, IG, and Kelvin waves, respectively.

Earth's radius a, which is absent in this 1D model. In this part, we define the MJO nondimensional wave number $\hat{k}$ as $2\pi/\hat{\lambda}$, where $\hat{\lambda}$ is the MJO nondimensional wavelength.
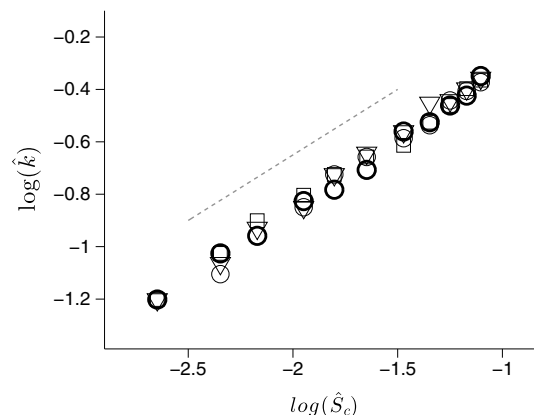
Figure 3 shows the power spectrum of $\hat{u}$ of the 1D model results. The most striking feature is the intense power density at low frequency and low positive wave number, which is associated with the MJO. The spectral power density is enhanced along the theoretical dispersion curves, which suggests that Kelvin waves and $n = 1$ Rossby and IG waves are present. The high-frequency IG waves are strongest among these equatorial waves. This may imply that the IG waves are important to the MJO. As this model keeps all the essential dynamics of the YI13 model, the governing mechanism of the MJO in this 1D model is the same as that of the 2D model. We will test the RCE scaling using this 1D model.

Figure 4 shows $\hat{k}$ and $\hat{S}_c$ in the 10-based logarithmic scale with different values of $\hat{\tau}_c$ and $\hat{R}_c$. Each marker represents one simulation result. All of the simulation results collapse onto one straight line with the slope of 0.54. The implication is that $\hat{k}$ does not depend on $\hat{\tau}_c$ and $\hat{R}_c$. An exponent of 0.50 would fit the RCE scaling, the dimensional form of which is

$$k \sim \left(\frac{S_c}{c}\right)^{1/2}. \tag{13}$$

Here k is has dimensions of 1/length, whereas in 4 and 5 k was dimensionless, having been scaled by the Earth radius a. Another difference is that S_c is per unit length and time in 13 and per unit area and time in 5. Comparing the 1D scaling 13 with the 2D scaling 5, we confirm that the size of convection R_c only enters by affecting the meridional length scale. Physically, the horizontal scale of the MJO is the scale within which positive-only convective heating balances the radiative cooling. This has two consequences. First, k increases (λ decreases) with S_c. Our interpretation is that weaker convection (larger S_c) can only balance radiation over a smaller scale, i.e., smaller MJOs (larger k). Second, k decreases with c. Our interpretation is that if the gravity wave travels faster, it can spread the convective heating to further distance, i.e., larger MJOs (smaller k).

4. Conclusion and Discussion

In this paper, we study what controls the MJO wave number by using the YI13 model and a 1D β-plane model. From our simulation results, we find a power law relation between k and the model parameters: S_c, c, and R_c. Then we derive a scaling for k based on the assumption that each MJO event is in RCE, and this RCE scaling argument explains our simulation results. This RCE scaling is consistent with the findings in YI13 that the positive-only convection produces the large-scale envelope of the MJO.

This success in simulating the MJO using both 1D and 2D models suggests that triggered convection might be important in simulating the MJO. With

Figure 4. The 1D scaling relation in a 10-based log-log plot. Each marker represents a simulation result. The simulation results with $\hat{R}_c = 0.4, 0.8, 1.6$ are labeled with squares, circles, and triangles. The simulation results with $\hat{\tau}_c = 0.2$ and 0.4 are labeled with thick and thin markers. The dashed line has a slope of 0.5.

only three nondimensional parameters, the 1D model is arguably the minimum model that includes all the essential recipes of the MJO—equatorial wave dynamics and self-excited, intermittent, and energetic convective events. Although there is not a moisture variable in our model, we do not exclude the role of moisture in the MJO. Only with moisture could triggered convection happen in the atmosphere. As a test of these low dimension models, we are simulating the MJO with a 3D moist GCM, in which triggered convection is applied.

One use of this study is to predict the MJO behavior in a different climate. In a warmer climate, convection is more vigorous (larger q_0) and dry static stability increases. As a result, S_c will decrease and c will increase. If R_c does not vary, k will decrease according to 5. Meanwhile, the number of convection events in each MJO event is constant in different climates. In a warmer climate, the MJO is stronger because the convective events are more vigorous. Our prediction is qualitatively consistent with the SPCAM simulations [*Arnold et al.*, 2013]. To test whether our scaling arguments could explain the SPCAM simulations quantitatively, we propose to run the SPCAM over a wide range of climates and quantify q_0, S_c, and c in the SPCAM simulations.

References

Andersen, J. A., and Z. Kuang (2012), Moist static energy budget of MJO-like disturbances in the atmosphere of a zonally symmetric aquaplanet, *J. Clim.*, *25*, 2782–2804.

Arnold, N. P., Z. Kuang, and E. Tziperman (2013), Enhanced MJO-like Variability at High SST, *J. Clim.*, *26*, 988–1001.

Bretherton, C. S., P. N. Blossey, and M. Khairoutdinov (2005), An energy-balance analysis of deep convective self-aggregation above uniform SST, *J. Atmos. Sci.*, *62*, 4273–4292.

Chen, S. S., R. A. Houze, and B. E. Mapes (1996), Multiscale variability of deep convection in realation to large-scale circulation in TOGA COARE, *J. Atmos. Sci.*, *53*, 1380–1409.

Emanuel, K., J. Neelin, and C. Bretherton (1994), On large-scale circulations in convecting atmospheres, *Q. J. R. Meteorol. Soc.*, *120*, 1111–1143.

Fuchs, Z., and D. J. Raymond (2002), Large-scale modes of a nonrotating atmosphere with water vapor and cloud–radiation feedbacks, *J. Atmos. Sci.*, *59*, 1669–1679.

Fuchs, Z., and D. J. Raymond (2005), Large-scale modes in a rotating atmosphere with radiative–convective instability and WISHE, *J. Atmos. Sci.*, *62*, 4084–4094.

Fuchs, Z., and D. J. Raymond (2007), A simple, vertically resolved model of tropical disturbances with a humidity closure, *Tellus, Ser. A*, *59*, 344–354.

Holloway, C. E., S. J. Woolnough, and G. M. S. Lister (2013), The effects of explicit versus parameterized convection on the MJO in a large-domain high-resolution tropical case study. Part I: Characterization of large-scale organization and propagation, *J. Atmos. Sci.*, *70*, 1342–1369.

Madden, R. A., and P. R. Julian (1972), Description of global-scale circulation cells in the tropics with a 40–50 day period, *J. Atmos. Sci.*, *29*, 1109–1123.

Madden, R. A., and P. R. Julian (1994), Observations of the 40–50-day tropical oscillation—A review, *Mon. Weather Rev.*, *122*, 814–837.

Maloney, E. D. (2009), The moist static energy budget of a com- posite tropical intraseasonal oscillation in a climate model, *J. Clim.*, *22*, 711–729.

Matsuno, T. (1966), Quasi-geostrophic motions in the equatorial area, *J. Meteorol. Soc. Jpn.*, *44*, 25–43.

Nakazawa, T. (1988), Tropical super clusters within intraseasonal variations over the western Pacific, *J. Meteorol. Soc. Jpn.*, *66*, 823–839.

Neelin, J. D., and J.-Y. Yu (1994), Modes of tropical variability under convective adjustment and the Madden–Julian oscillation. Part I: Analytical theory, *J. Atmos. Sci.*, *51*, 1876–1894.

Raymond, D. J., and Z. Fuchs (2009), Moisture modes and the Madden–Julian oscillation, *J. Clim.*, *22*, 3031–3046.

Sobel, A. H., J. Nilsson, and L. M. Polvani (2001), The weak temperature gradient approximation and balanced tropical moisture waves, *J. Atmos. Sci.*, *58*, 3650–3665.

Yang, D., and A. P. Ingersoll (2013), Triggered convection, gravity waves, and the MJO: A shallow-water model, *J. Atmos. Sci.*, *70*, 2476–2486.

Zhang, C. (2005), Madden-Julian Oscillation, *Rev. Geophys.*, *43*, RG2003, doi:10.1029/2004RG000158.

Zuluaga, M. D., and H. A. Robert (2013), Evolution of the population of precipitating convective systems over the equatorial Indian Ocean in active phases of the Madden-Julian Oscillation, *J. Atmos. Sci.*, *70*, 2713–2725, doi:10.1175/JAS-D-12-0311.1.

YANG AND INGERSOLL

1064